Polarization Inversion with Parity–Time-Reversal–Duality Symmetric Scatterers

Roee Geva,[1] Mário G. Silveirinha,[2] and Raphael Kastner[1]
[1]Tel Aviv University, Tel Aviv, 69978 Israel
[2]University of Lisbon and Instituto de Telecomunicações, Avenida Rovisco Pais 1, Lisboa, 1049-001 Portugal

(Received 23 January 2025; revised 19 May 2025; accepted 1 July 2025; published 30 July 2025)

We demonstrate, both theoretically and experimentally, that arbitrary scatterers preserving parity–time-reversal–duality ($\mathcal{P}\cdot\mathcal{T}\cdot\mathcal{D}$) symmetry inherently produce a backscattered wave whose electric field is the mirror-symmetric counterpart of the incident electric field, up to an amplitude factor, with respect to the system's characteristic mirror plane. Specifically, we establish that a general elliptically polarized wave, when reflected from such structures, exhibits a polarization state related to the polarization ellipse of the incident wave by a parity transformation. Notably, a circularly polarized wave reflects with spin angular momentum opposite to that of the incident field, in stark contrast to reflection from conventional conducting objects. These findings enable several applications such as reflective polarizers and spin-selective devices.

DOI: 10.1103/7928-bf5j

Electromagnetic and photonic systems that are invariant under parity ($\mathcal{P}$), time-reversal ($\mathcal{T}$), and duality ($\mathcal{D}$) can support propagation without backscattering, even in complex environments [1,2]. This remarkable behavior stems from the fact that $\mathcal{P}\cdot\mathcal{T}\cdot\mathcal{D}$ symmetry enforces antisymmetry in the system's scattering matrix when expressed in the $\mathcal{P}\cdot\mathcal{T}\cdot\mathcal{D}$ basis, $\mathbf{S}=-\mathbf{S}^T$. This antisymmetry is a direct consequence of the antilinear nature of the operator $\tilde{\mathcal{T}}=\mathcal{P}\cdot\mathcal{T}\cdot\mathcal{D}$, which behaves analogously to a fermionic time-reversal operator with $\tilde{\mathcal{T}}^2=-\mathbf{1}$ [1,3].

The antisymmetric scattering matrix ensures that an electromagnetic wave incident on $\mathcal{P}\cdot\mathcal{T}\cdot\mathcal{D}$-symmetric structures cannot undergo reflection in certain propagation channels, enabling reflectionless transport in systems with an odd number of bidirectional modes [1]. This unique property opens new avenues for designing electromagnetic devices that leverage robust unidirectional propagation and efficient energy transfer [1,2,4–7]. Crucially, these reflectionless characteristics persist even in the presence of non-Hermitian effects, such as material dissipation [8]. Additionally, $\mathcal{P}\cdot\mathcal{T}\cdot\mathcal{D}$-symmetric systems are often associated with nontrivial topological phases, further enhancing their potential for advanced electromagnetic applications [1,8–12].

Previous studies have primarily focused on wave propagation in $\mathcal{P}\cdot\mathcal{T}\cdot\mathcal{D}$-invariant waveguides, e.g., [1,2,5,7]. In this Letter, we explore the scattering of waves by $\mathcal{P}\cdot\mathcal{T}\cdot\mathcal{D}$-invariant objects embedded in free space. Remarkably, we demonstrate that $\mathcal{P}\cdot\mathcal{T}\cdot\mathcal{D}$ invariance imposes unique characteristics on the scattered fields. Specifically, we show that the wave backscattered by any $\mathcal{P}\cdot\mathcal{T}\cdot\mathcal{D}$-invariant scatterer is always polarized along a direction that differs by a mirror transformation from the incident field. We refer to this phenomenon as polarization inversion. Furthermore, we reveal that, unlike conventional materials, $\mathcal{P}\cdot\mathcal{T}\cdot\mathcal{D}$-invariant objects reverse the spin angular momentum of the wave, causing the incident and backscattered fields to rotate in opposite directions. In addition, we demonstrate that our theory includes as a particular case the well-known Kerker condition [13–15]. Rotationally symmetric nonreflective structures [16], however, are a complementary case.

$\mathcal{P}\cdot\mathcal{T}\cdot\mathcal{D}$-symmetric systems are known to eliminate reflections within a given incident mode [1]. Specifically, for a given arbitrary incident mode $\mathbf{f}^+(\mathbf{r})$ the theory of Ref. [1] guarantees that this wave cannot backscatter into the "companion" mode defined as

$$\tilde{\mathbf{f}}(\mathbf{r})=\tilde{\mathcal{T}}\cdot\mathbf{f}^+(\mathbf{r}'),\qquad \mathbf{r}'=\mathbf{V}\cdot\mathbf{r},$$

where $\tilde{\mathcal{T}}$ is the operator obtained by the composition of parity, time-reversal, and duality operators:

$$\tilde{\mathcal{T}}=\mathcal{P}\cdot\mathcal{T}\cdot\mathcal{D}=\begin{pmatrix}0 & \eta_0\mathbf{V}\\ -\eta_0^{-1}\mathbf{V} & 0\end{pmatrix}\mathcal{K}. \tag{1}$$

Here, η_0 is the free-space impedance, $\mathcal{K}$ is the complex conjugation operator, and $\mathbf{V}$ is the y-coordinate inversion operator

$$\mathbf{V}=\begin{pmatrix}1 & 0 & 0\\ 0 & -1 & 0\\ 0 & 0 & 1\end{pmatrix}. \tag{2}$$

It is implicit that the mirror plane is the x–z plane. A reciprocal physical platform is invariant under the $\tilde{\mathcal{T}}$

transformation if the material response at a certain point (x, y, z) is related to the material response at the mirror-symmetric point $(x, -y, z)$ by a duality transformation. For example, in systems formed by isotropic dielectrics, the $\tilde{\mathcal{T}}$ symmetry requires that the relative permittivity and permeability are linked as $\epsilon(x, y, z) = \mu(x, -y, z)$.

Let us assume that the incident wave is a plane wave that illuminates the object along the direction $\hat{\mathbf{r}}_i = \hat{\mathbf{z}}$.

$$\mathbf{f}^+ = \begin{pmatrix} \mathbf{e}_0^+ \\ \mathbf{h}_0^+ \end{pmatrix} e^{-\jmath k_0 \hat{\mathbf{r}}_i \cdot \mathbf{r}}, \qquad \mathbf{h}_0^+ = \frac{\hat{\mathbf{r}}_i}{\eta_0} \times \mathbf{e}_0^+. \tag{3}$$

In the above, $k_0 = \omega/c$ is the free-space wave number. Then, from Eqs. (1) and (2), the companion mode is [1]

$$\tilde{\mathbf{f}} = \begin{pmatrix} \tilde{\mathbf{E}} \\ \tilde{\mathbf{H}} \end{pmatrix} = \begin{pmatrix} \eta_0 \mathbf{V} \cdot \mathbf{h}^{+*}(\mathbf{r}') \\ -\eta_0^{-1} \mathbf{V} \cdot \mathbf{e}^{+*}(\mathbf{r}') \end{pmatrix} = \begin{pmatrix} \tilde{\mathbf{e}}_0 \\ \tilde{\mathbf{h}}_0 \end{pmatrix} e^{+\jmath k_0 (\mathbf{V} \cdot \hat{\mathbf{r}}_i) \cdot \mathbf{r}} \tag{4}$$

Note that $\tilde{\mathbf{f}}$ describes a plane wave that propagates along the backscatter direction $-\mathbf{V} \cdot \hat{\mathbf{r}}_i = -\hat{\mathbf{z}}$, i.e., it describes a particular mode of the reflected field with an electric field polarized along $\tilde{\mathbf{e}}_0 = \mathbf{V} \cdot (\hat{\mathbf{z}} \times \mathbf{e}_0^{+*})$.

The $\mathcal{P} \cdot \mathcal{T} \cdot \mathcal{D}$ theory ensures that the backscattered field $\mathbf{E}^-$ has a trivial projection over the companion mode, i.e., that $\tilde{\mathbf{e}}_0^* \cdot \mathbf{E}^- = 0$. Noting that the vectors $\tilde{\mathbf{e}}_0$ and $\mathbf{V} \cdot \mathbf{e}_0^+$ are orthogonal $[(\mathbf{V} \cdot \mathbf{e}_0^+)^* \cdot \tilde{\mathbf{e}}_0 = 0]$, they can form basis in the x–y plane (Fig. 1). It then becomes clear that the backscattered field must be aligned with $\mathbf{V} \cdot \mathbf{e}_0^+$, i.e., $\mathbf{E}^- \sim \mathbf{V} \cdot \mathbf{e}_0^+$. Thus, up to an amplitude factor, the reflected field is related to the incident field by a mirror transformation.

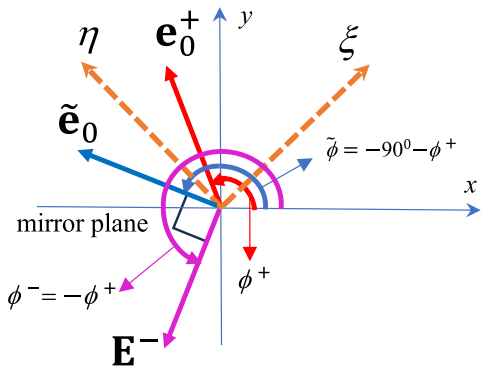

FIG. 1. Effect of applying the $\mathcal{P} \cdot \mathcal{T} \cdot \mathcal{D}$ operator on a linear polarized incident polarization state $\mathbf{e}_0^+$. The polarization direction is mirror-transformed by the $\mathcal{P} \cdot \mathcal{T} \cdot \mathcal{D}$ object. In the special cases of $\phi^+ = 45°, 135°$ defining the coordinates (ξ, η), the directions of $\mathbf{e}_0^+$ and $\tilde{\mathbf{e}}_0$ coincide. These are the polarization "eigenstates" of the $\mathcal{P} \cdot \mathcal{T} \cdot \mathcal{D}$ operation, for which the co-polarized reflection coefficients vanish. Because a $\mathcal{P} \cdot \mathcal{T} \cdot \mathcal{D}$ system does not allow backscatter towards the $\tilde{\phi}^+$ direction, the reflected wave $\mathbf{E}^-$ must be perpendicular to $\tilde{\mathbf{e}}_0$. Its phase and amplitude depend on the coefficient a in Eq. (5).

The geometrical relationship between the incident electric field $(\mathbf{e}_0^+)$, the electric field of the companion mode $(\tilde{\mathbf{e}}_0)$, and the backscattered field is depicted in Fig. 1 for the case of a linearly polarized wave. Notably, the electric field of the companion mode is parallel to the mirror-transformed magnetic field of the incident wave. Furthermore, the backscattered electric field is orthogonal to the electric field of the companion mode. The incident electric field and the backscattered field, apart from a scaling factor, are related by a parity transformation with respect to the system's mirror plane ($y = 0$).

In $\mathcal{P} \cdot \mathcal{T} \cdot \mathcal{D}$-symmetric systems, an incident mode $(\mathbf{f}^+)$ produces no reflections in the companion mode $(\tilde{\mathbf{f}})$. However, it may backscatter into other orthogonal modes if these are supported by the system. This is the case in our problem, where two independent propagation channels are associated with the same physical direction of propagation due to the polarization degree of freedom. In general, total suppression of backscattering can be guaranteed for a suitable excitation of the system only when the number of independent physical channels is odd [1].

Let us write the incident electric field in terms of its components $\mathbf{e}_0^+ = e_{0x}^+ \hat{\mathbf{x}} + e_{0y}^+ \hat{\mathbf{y}}$. Then, the backscattered electric field must be of the type

$$\mathbf{E}^- = a(e_{0x}^+ \hat{\mathbf{x}} - e_{0y}^+ \hat{\mathbf{y}}), \tag{5}$$

where $|a| \leq 1$ depends on the transmission and absorption levels. For an arbitrary incident polarization, the polarization ellipse of the reflected wave differs (apart from a scale factor) from the polarization ellipse of the incident wave by a mirror transformation with respect to the y axis. In particular, for elliptically polarized waves, the absolute physical sense of rotation of the polarization ellipse is reversed compared with the sense of rotation of the incident field. In fact, one of the most remarkable features of $\mathcal{P} \cdot \mathcal{T} \cdot \mathcal{D}$ scatterers is that they flip the spin angular momentum of a wave.

For example, suppose that the incident wave is circularly polarized to the right (RCP), corresponding to an incident field with $e_{0y}^+ = -\jmath e_{0x}^+$. The corresponding spin angular momentum of the wave [17,18], defined as $\boldsymbol{\sigma} = -\jmath(\mathbf{E} \times \mathbf{E}^* / \mathbf{E} \cdot \mathbf{E}^*)$, is oriented along the $+z$-direction $(\boldsymbol{\sigma}^+ = \hat{\mathbf{z}})$, as expected. Strikingly, upon reflection on the scatterer, the spin angular momentum becomes $\boldsymbol{\sigma}^- = -\hat{\mathbf{z}}$, which also corresponds to an RCP reflected wave. A related property (preservation of electromagnetic helicity) was previously discussed in [14] for general dual $(\mathcal{D})$ symmetric systems.

Thus, unlike conventional scatterers (e.g., metallic or dielectric mirrors), a $\mathcal{P} \cdot \mathcal{T} \cdot \mathcal{D}$ structure reverses the absolute sense of rotation of the scattered electric field compared to the incident field. Note that for a conventional

scatterer, the spin angular momentum direction for the backscattered wave is the same for both the incident and reflected waves, so that an RCP wave is reflected into a left-circularly polarized (LCP) wave, and vice versa.

Of particular interest are the cases of the "eigenstates" $\phi^+ = 45°, 135°$, corresponding to a linearly polarized incident field aligned with the companion mode, i.e., the reflected wave $\mathbf{E}^-$ is perpendicular to $\mathbf{e}_0^+$. (see Fig. 1). In this case, reflection into the co-polarized mode is forbidden, meaning that the backscattered field consists exclusively of the cross-polarized wave. The axes of the eigenstates are labeled as ξ and η in Fig. 1. For an incident field polarized along ξ, no co-polarized reflection will be observed; however, the wave can be fully or partially reflected into the η-polarized (cross-polarized) component.

The described results apply to general $\mathcal{P}\cdot\mathcal{T}\cdot\mathcal{D}$ symmetric scatterers. The scattered field for a generic object can be written as

$$\mathbf{E}^s(\mathbf{r}) = \mathbf{L}(\hat{\mathbf{r}}, \hat{\mathbf{r}}_i)\cdot\mathbf{E}_0\frac{e^{-\jmath k_0 r}}{4\pi r}. \tag{6}$$

The formula is valid in the far-field region, where the scattered wave is approximately spherical. In the above $\mathbf{E}_0$ is the incident field on the center of the object, $\hat{\mathbf{r}}$ is the observation direction, and $\hat{\mathbf{r}}_i$ is the propagation direction of the incoming plane wave. Furthermore, $\mathbf{L}(\hat{\mathbf{r}}, \hat{\mathbf{r}}^i)$ is a matrix with units of length that determines the directional and polarization properties of the scattered field. For convenience, we define $\mathbf{E}^-(\hat{\mathbf{r}}, \hat{\mathbf{r}}_i, \mathbf{E}_0) \equiv \mathbf{L}(\hat{\mathbf{r}}, \hat{\mathbf{r}}_i)\cdot\mathbf{E}_0$.

The $\mathcal{P}\cdot\mathcal{T}\cdot\mathcal{D}$ symmetry requires that, for any physical channel i, the corresponding diagonal scattering matrix element vanishes, $S_{ii} = 0$ [1]. For incidence along $\hat{\mathbf{r}}_i$, the companion mode propagates along $\hat{\mathbf{r}} = -\mathbf{V}\cdot\hat{\mathbf{r}}_i$ and is polarized along $\mathbf{V}\cdot(\hat{\mathbf{r}}_i \times \mathbf{E}_0^*)$ [see (4)]. It follows that the condition $S_{ii} = 0$ imposes the requirement $[\mathbf{V}\cdot(\hat{\mathbf{r}}_i \times \mathbf{E}_0^*)]^*\cdot\mathbf{E}^- = 0$. It is implicit here and in the formulas below that $\mathbf{E}^-$ is evaluated at $\hat{\mathbf{r}} = -\mathbf{V}\cdot\hat{\mathbf{r}}_i$. Equivalently, $((\mathbf{V}\cdot\hat{\mathbf{r}}_i)\times(\mathbf{V}\cdot\mathbf{E}_0))\cdot\mathbf{E}^- = 0$. This condition can only be satisfied if the scattered field obeys: $\mathbf{E}^- \sim \mathbf{V}\cdot\mathbf{E}_0$. In particular, when the propagation direction of the incident plane wave lies in the mirror plane, so that $\hat{\mathbf{r}}_i$ is in the $y = 0$ plane, it follows that the backscattered field is polarized along a direction that is mirror symmetric with respect to the incident field: $\mathbf{E}^-(-\hat{\mathbf{r}}_i, \hat{\mathbf{r}}_i, \mathbf{E}_0) \sim \mathbf{V}\cdot\mathbf{E}_0$. Thus, $\mathcal{P}\cdot\mathcal{T}\cdot\mathcal{D}$ symmetric objects inherently constrain the polarization of the backscattered field to be mirror symmetric with respect to the incident field polarization, independent of the material geometry or the detailed material response. Eigenpolarized incident field can then be defined as the case where $(\mathbf{V}\cdot\mathbf{E}_0)\cdot\mathbf{E}_0^* = 0$, corresponding to a vanishing copolarized reflected wave.

In the Supplemental Material [19], we present a more rigorous and general derivation of this result, which applies also to generalized non-Hermitian $\mathcal{P}\cdot\mathcal{T}\cdot\mathcal{D}$ systems, where $\epsilon(x, y, z) = \mu(x, -y, z)$, with $\epsilon = \epsilon' - \jmath\epsilon''$ and $\mu = \mu' - \jmath\mu''$, with the imaginary parts representing dissipative material responses. The present analysis, though, is based on the Hermitian case developed in [1].

Our theory encompasses, as a particular case, the celebrated Kerker condition [13–15], which states that spherical objects invariant under duality symmetry do not scatter in the backward direction. Indeed, for such objects, the symmetry plane can be oriented along an arbitrary direction, ensuring that both the copolarized and cross-polarized components of the backscattered field vanish. Another interesting example of a $\mathcal{P}\cdot\mathcal{T}\cdot\mathcal{D}$-symmetric system is the class of soft-hard metasurfaces introduced by Kildal [21,22].

It is worth noting that our theory can be readily extended to electronic systems protected by time-reversal symmetry. In this case, an incoming plane wave with a given spin cannot backscatter into the companion mode with opposite spin. This phenomenon is widely discussed in the context of the spin Hall effect and topological insulators [3].

In this Letter, we focus on objects of finite size. Specifically, we have designed a planar reflective polarizer with the geometry shown in Fig. 2. The scatterer consists of a perfect electric conductor (PEC)-like section (which can be modeled as, $\epsilon \to -\infty, \mu = 1$) and a perfect magnetic conductor (PMC)-like section ($\mu \to -\infty, \epsilon = 1$). The two sections are electromagnetic dual and linked by mirror symmetry, ensuring PTD invariance. In the Supplemental Material [19], we present

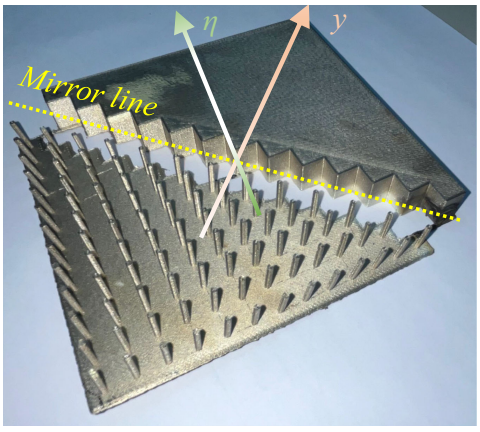

FIG. 2. Photograph of the fabricated $\mathcal{P}\cdot\mathcal{T}\cdot\mathcal{D}$ scatterer. The top-right region is metallic, providing a PEC-like response, while the bottom-left region is an artificial magnetic conductor (AMC) that behaves as a PMC at the design frequency ($f \approx 7.5$ GHz). For practical reasons, the PEC and AMC regions are separated by a small air gap. The AMC section consists of an array of square pins with a height of 11 mm and a cross-sectional area of 1.5×1.5 mm^2, arranged in a 7.5×7.5 mm^2 grid. The structure was fabricated additively using a plastic substrate coated with thin layers of silver and nickel. The axes follow the definitions in Fig. 1.

a detailed numerical analysis of related PTD-symmetric objects [20] where the PMC region is treated as an idealized magnetic conductor.

In the prototype in Fig. 2, the artificial magnetic conductor (PMC-like) region is realized using a bed-of-nails configuration [23–26]. The prototype was fabricated using additive manufacturing, with a 3D printer used to create a plastic structure that was subsequently coated with a thin layer of metal to achieve the desired electromagnetic properties. For comparison, a fully-PEC structure of the same dimensions was also fabricated. Both structures were tested in an anechoic chamber.

To evaluate the response of the artificial magnetic conductor (AMC), we measured the backscattered field as a function of frequency for an incident wave polarized along the ξ and η directions. At the design frequency (7.5 GHz), where the bed of nails is expected to behave as a PMC, the copolarization component of the reflected wave is predicted to vanish.

Figure 3(a) shows the measured backscattered field over the 5–11 GHz frequency range. A pronounced null is observed at the AMC's design frequency, confirming the nonreflective property of the $\mathcal{P}\cdot\mathcal{T}\cdot\mathcal{D}$-symmetric structure for the two eigenpolarizations of the scatterer.

The null in the co-polarized backscattered field occurs at a frequency of $f = 7.57$ GHz. For comparison, the plot also includes the response of a reference PEC plate of the same size, which exhibits high reflection across the entire

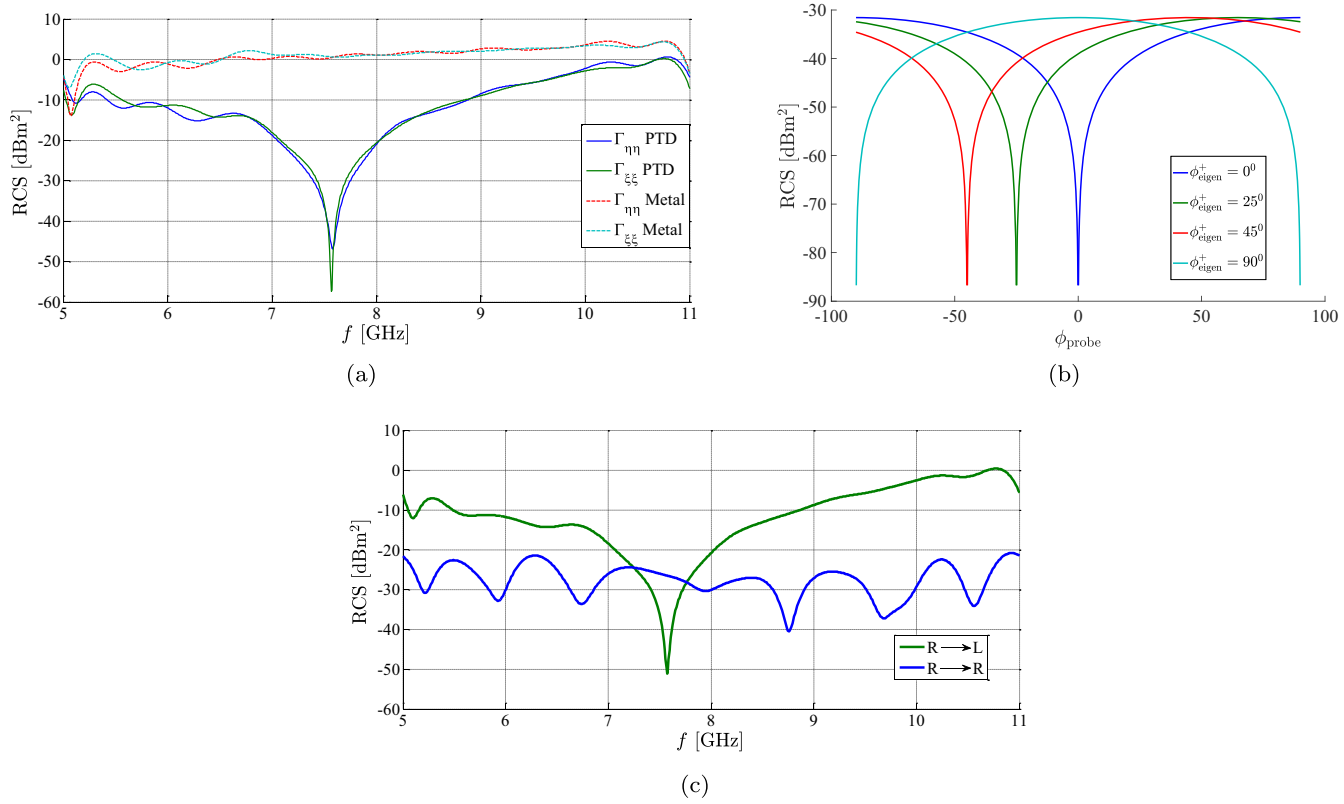

FIG. 3. (a) Measured copolarized backscattered field as a function of frequency. The incident electric field is either aligned with the ξ or η axis. At the AMC center frequency of $f = 7.57$ GHz the backscattered field displays a deep null. For comparison we also depict the copolarized backscattered field for a PEC plate. (b) Measured backscattered field as a function of the orientation of the receiving probe, denoted ϕ_{probe}, for four different incident polarizations at $f = 7.57$ GHz. The angles $\phi^{+}_{\text{eigen}} = \phi^{+} - 135°$, $\tilde{\phi}_{\text{eigen}} = \tilde{\phi} - 135°$, and ϕ_{probe} are defined with respect to the η axis in Fig. 1. The figure confirms that, in all cases, the backscattered electric field undergoes a mirror transformation. The measured pattern exhibits a deep null when the receiving probe is oriented parallel to the field of the companion mode at $\phi_{\text{probe}} = \tilde{\phi}^{+}_{\text{eigen}} \equiv -\phi^{+}_{\text{eigen}}$. Blue line: Incidence at the eigenpolarization along the η axis ($\phi^{+}_{\text{eigen}} = 0°$). The null occurs at the same polarization as the incidence, qualitatively similar to the simulations in Fig. S2(a) in [19] although for a different geometry. Green line: Incidence at $\phi^{+}_{\text{eigen}} = 25°$, with the null observed at $\tilde{\phi}_{\text{eigen}} = -25°$. Red line: Incidence at $\phi^{+}_{\text{eigen}} = 45°$, showing a null at $\tilde{\phi}_{\text{eigen}} = -45°$, qualitatively similar to Fig. S2(b) in [19]. Cyan line: Incidence at the eigenpolarization along the η axis ($\phi^{+}_{\text{eigen}} = 90°$), with the null occurring at the same polarization. (c) Measured right- and left-circular polarization components of the backscattered field as a function of frequency for right-handed circular polarization incidence. Across most of the frequency spectrum, the scattering behavior resembles that of a PEC mirror, with dominant right-to-left polarization conversion (green curve). However, near the design frequency of the AMC, the right-to-left conversion is strongly suppressed, and the right-circular incident polarization is fully converted into a right-circular reflected polarization (blue curve), corresponding to a reversal of the spin angular momentum.

frequency range. Additionally, the numerically simulated response of the same system is provided in the Supplemental Material, demonstrating a qualitatively similar result [19].

The effect of polarization inversion is experimentally confirmed in Fig. 3(b). In the figure, the orientations of the incident field ($\phi^{+}_{\text{eigen}} = \phi^{+} - 135°$) and measurement probe orientation ϕ_{probe} are defined with respect to the eigenpolarization axis η indicated in Figs. 1 and 2. As seen in Fig. 3(b), the polarization-resolved backscattered field exhibits nulls when the probe is aligned along the direction of the companion mode ($\tilde{\phi}_{\text{eigen}} = \tilde{\phi} - 135°$), i.e., when the probe orientation satisfies $\phi_{\text{probe}} = \tilde{\phi}_{\text{eigen}} = -\phi^{+}_{\text{eigen}}$. The energy is deflected into the orthogonal polarization state. The curves follow roughly the projection of the cross-polarized component on the measured polarization. These results qualitatively align with the simulations presented in Figs. S2(a)–S2(b) in [19], although corresponding to a different object.

Figure 3(c) shows the experimentally measured RCP and LCP polarization-resolved components of the backscattered field as a function of frequency for an incident wave that is right-circularly polarized. As observed, across most of the frequency range, the RCP-to-LCP polarization conversion dominates (green line), consistent with the behavior of conventional metallic and dielectric mirrors, which preserve the spin angular momentum of the wave, i.e., the absolute direction of rotation of the field with respect to a fixed reference frame.

Remarkably, near the AMC center frequency (7.57 GHz), the RCP-to-LCP polarization component exhibits a deep null. Consistent with the general theory of scattering by $\mathcal{P}\cdot\mathcal{T}\cdot\mathcal{D}$ symmetric objects, the backscattered field is dominated by the RCP-to-RCP polarization component (blue curve). This result experimentally confirms that $\mathcal{P}\cdot\mathcal{T}\cdot\mathcal{D}$ symmetric objects inherently provide a reversal of the spin angular momentum of the wave, despite being formed from fully reciprocal materials. This unique property has exciting potential applications in the design of objects with exotic scattering signatures.

In conclusion, we unveiled the unique scattering properties of $\mathcal{P}\cdot\mathcal{T}\cdot\mathcal{D}$-symmetric objects, highlighting their ability to enforce polarization inversion and reverse the spin angular momentum of backscattered waves. These results go beyond conventional scattering paradigms, revealing that the interplay of parity, time-reversal, and duality symmetries imposes strict constraints on the polarization and angular momentum of scattered fields, independent of material specifics or geometric details.

We have experimentally validated these effects, confirming not only the robustness of the theoretical predictions but also establishing a foundation for engineering novel photonic devices with tailored scattering signatures. By harnessing the inherent symmetry properties of $\mathcal{P}\cdot\mathcal{T}\cdot\mathcal{D}$ systems, this Letter opens avenues for applications in polarization control, spin-selective devices, and advanced wave manipulation technologies.

Acknowledgments—This work is partially supported by the Israel Science Foundation (ISF) under Contract No. 1173/24, by the IET, by the Simons Foundation under the Award No. SFI-MPS-EWP-00008530-10 (Simons Collaboration in Mathematics and Physics, "Harnessing Universal Symmetry Concepts for Extreme Wave Phenomena"), and by FCT/Portuguese Ministry of Education, Science and Innovation (MECI) through national funds and when applicable co-funded EU funds under UID/50008: Instituto de Telecomunicações.

Data availability—The data that support the findings of this Letter are not publicly available upon publication because it is not technically feasible and/or the cost of preparing, depositing, and hosting the data would be prohibitive within the terms of this research project. The data are available from the authors upon reasonable request.

[1] M. G. Silveirinha, Phys. Rev. B **95**, 035153 (2017).
[2] W.-J. Chen, Z.-Q. Zhang, J.-W. Dong, and C. T. Chan, Nat. Commun. **6**, 8183 (2015).
[3] S.-Q. Shen, *Topological Insulators*, Series in Solid State Sciences Vol. 174 (Springer, Berlin, 2012).
[4] D. E. Fernandes and M. G. Silveirinha, Phys. Rev. Appl. **12**, 014021 (2019).
[5] D. J. Bisharat and D. F. Sievenpiper, Phys. Rev. Lett. **119**, 106802 (2017).
[6] D. J. Bisharat and D. F. Sievenpiper, Laser Photonics Rev. **13**, 1900126 (2019).
[7] E. Martini, M. G. Silveirinha, and S. Maci, IEEE Trans. Antennas Propag. **67**, 1035 (2019).
[8] R. P. Câmara, T. G. Rappoport, and M. G. Silveirinha, Phys. Rev. B **109**, L241406 (2024).
[9] A. B. Khanikaev, S. H. Mousavi, W.-K. Tse, M. Kargarian, A. H. MacDonald, and G. Shvets, arXiv:1204.5700.
[10] C. He, X.-C. Sun, X.-P. Liu, M.-H. Lu, Y. Chen, L. Feng, and Y.-F. Chen, Proc. Natl. Acad. Sci. U.S.A. **113**, 4924 (2016).
[11] S. Lannebère and M. G. Silveirinha, Nanophotonics **8**, 1387 (2019).
[12] X. Cui, R.-Y. Zhang, Z.-Q. Zhang, and C. T. Chan, Phys. Rev. Lett. **129**, 043902 (2022).
[13] M. Kerker, D.-S. Wang, and C. Giles, J. Opt. Soc. Am. A **73**, 765 (1983).
[14] I. Fernandez-Corbaton, X. Zambrana-Puyalto, N. Tischler, X. Vidal, M. L. Juan, and G. Molina-Terriza, Phys. Rev. Lett. **111**, 060401 (2013).
[15] J.-M. Geffrin, B. García-Cámara, R. Gómez-Medina, P. Albella, L. S. Froufe-Pérez, C. Eyraud, A. Litman, R. Vaillon, F. González, M. Nieto-Vesperinas *et al.*, Nat. Commun. **3**, 1171 (2012).
[16] N. Mohammadi Estakhri, N. Engheta, and R. Kastner, Phys. Rev. Lett. **124**, 033901 (2020).

[17] K. Y. Bliokh, A. Y. Bekshaev, and F. Nori, Nat. Commun. **5**, 3300 (2014).
[18] K. Y. Bliokh, D. Smirnova, and F. Nori, Science **348**, 1448 (2015).
[19] See Supplemental Material at http://link.aps.org/supplemental/10.1103/7928-bf5j for (Secs. A, B, C) for derivation of the constraints for the directional pattern of the fields scattered by generalized non-Hermitian $\mathcal{P}\cdot\mathcal{T}\cdot\mathcal{D}$ objects, Sec. D for full-wave simulations of the back-scattered field for an example from [20], and for the experimental setup discussed in the main text. The Supplemental Material also contains Ref. [1].
[20] M. Fazeli, K. Moralic, and M. J. Mencagli, in *2021 IEEE International Symposium on Antennas and Propagation and USNC-URSI Radio Science Meeting, Piscataway, New Jersey* (2021), 10.1109/APS/URSI47566.2021.
[21] P.-S. Kildal, Electron. Lett. **24**, 168 (1988).
[22] P.-S. Kildal, IEEE Trans. Antennas Propag. **38**, 1537 (1990).
[23] R. J. King, D. V. Thiel, and K. S. Park, IEEE Trans. Antennas Propag. **31**, 471 (1983).
[24] D. Sievenpiper, L. Zhang, R. F. J. Broas, N. G. Alexopolous, and E. Yablonovitch, IEEE Trans. Microwave Theory Tech. **47**, 2059 (1999).
[25] M. G. Silveirinha, C. A. Fernandes, and J. R. Costa, IEEE Trans. Antennas Propag. **56**, 405 (2008).
[26] A. Polemi, S. Maci, and P. S. Kildal, IEEE Trans. Antennas Propag. **59**, 904 (2011).